Hysteresis effects in spin systems with quenched disorder

Varsha Banerjee[1] and Sanjay Puri[2]
[1]*Department of Physics, Indian Institute of Technology, Hauz Khas, New Delhi 110016, India*
[2]*School of Physical Sciences, Jawaharlal Nehru University, New Delhi 110067, India*
(Received 31 May 2000; published 19 January 2001)

We present detailed numerical results for hysteresis effects in spin-glass systems. In particular, we focus on the dependence of hysteresis loop area on (a) disorder amplitude and (b) frequency of the applied magnetic field.

DOI: 10.1103/PhysRevE.63.026106 PACS number(s): 05.50.+q, 05.45.−a

I. INTRODUCTION

There has been intense research interest in the static and dynamical properties of spin glasses, which consist of magnetic impurities randomly placed in a host lattice [1–4]. These systems exhibit many properties analogous to those of structural glasses, e.g., slow relaxation, multiplicity of metastable states, etc. However, the physical origins of these properties are considerably different. In structural glasses, slow dynamics results from the trapping of particles in cages comprised of other particles. In spin glasses, slow evolution results from the effects of quenched disorder and frustration.

Experimental observations on spin glasses are usually interpreted in terms of phenomenological models with complicated free-energy landscapes, having deep valleys separated by randomly distributed barriers. This complex free-energy landscape leads to frequent trapping in local minima and the consequent breakdown of ergodicity in phase space, i.e., the system cannot access all states over the duration of a typical laboratory experiment. Because of the long time scales involved in spin-glass dynamics, most experimental systems should be understood as being effectively nonequilibrium systems.

An important nonequilibrium property of spin systems, in general (and spin glasses, in particular) is that of magnetic hysteresis. Typically, when an oscillating magnetic field is applied to an ordinary spin system, the response is delayed—leading to hysteresis effects. The magnitude of hysteresis is determined by the competition between experimental time scales (measured by the inverse frequency of the applied perturbation) and the spin relaxation time scale. The phenomenon of hysteresis has received considerable attention in the context of both pure and disordered spin systems, which we will review shortly.

In this paper, we focus upon hysteresis effects in spin-glass systems. We will consider two relevant cases, i.e., (a) weak-disorder limit, where the system is in the paramagnetic phase, and (b) strong disorder limit, where the system is in the spin-glass phase. We have already remarked that relaxation in disordered systems is characterized by a wide spectrum of relaxation times. Thus, the hysteretic response in these systems will be determined by a competition between the experimental time scale (inverse frequency) and a multitude of internal time scales. This problem has been the subject of some preliminary studies, which we discuss later.

This paper is organized as follows. In Sec. II, we provide a brief overview of the results known in the context of hysteresis in spin systems. In Sec. III, we discuss the soft-spin Sherrington-Kirkpatrick (SK) model and its dynamics. The detailed numerical results obtained from our simulations are presented in Sec. III. In Sec. IV, we present a discussion and summary of our results.

II. OVERVIEW OF KNOWN RESULTS

As we have remarked earlier, hysteresis effects in spin systems have been extensively studied in the literature. Let us briefly review some of the known results in this context.

A. Pure spin systems

In early work, Agarwal and Shenoy [5] formulated general conditions for the existence and nature of hysteresis loops, elucidating the role of various relevant time scales. An important work in the context of our present discussion is due to Jung *et al.* [6], who studied the hysteretic response of a single, continuous spin in a bistable potential. The loop area is perhaps the most important quantitative characteristic of the hysteresis loop as it is proportional to the heat dissipated during a field cycle. Jung *et al.* obtained an analytical expression for the loop area at small frequencies, i.e.,

$$A(\omega,h_0)=A(0,h_0)+a\,\omega^{2/3}(h_0^2-h_c^2)^{1/3}, \tag{1}$$

where $A(\omega,h_0)$ denotes the loop area for an external magnetic field $h_0\cos(\omega t)$; and a,h_c are constants. Jung *et al.* also verified their analytical result, both numerically and experimentally. Studies of the single-spin dynamics can also be thought of as a mean-field limit of the coupled-spin dynamics we will discuss subsequently,

Bose and Sarkar [7,8] extended the work of Jung *et al.* [6] in two important directions. First, they analytically obtained area-scaling laws valid for an extended region of (h_0,ω) values [7]. Secondly, they studied the effects of thermal noise on area-scaling laws and the dynamical symmetry-breaking transition [8].

The next class of studies we discuss involves interactng spin systems. In early work, Rao *et al.* [9] numerically studied hysteresis loops in interacting spin systems at temperatures below the ordering temperature. They considered two different cases: (a) Ising model with Monte Carlo (MC) kinetics, for which they obtained qualitative results. (b) Langevin studies of the time-dependent Ginzburg-Landau (TDGL)

model with $O(n)$ symmetry in the limit $n \to \infty$. For this model, their numerical results for low freqeuncies suggested an area-scaling law $A(\omega,h_0) \sim \omega^{1/3} h_0^{2/3}$. Subsequently, Dhar and Thomas [10] analytically studied case (b) above and obtained the result $A(\omega,h_0) \sim \omega^{1/2} h_0^{1/2}$—at variance with the numerical results of Rao *et al.* [9].

More extensive MC simulations of the Ising model in an oscillating field were conducted by Lo and Pelcovits [11]. Furthermore, Sengupta *et al.* [12] also studied this problem through a cell dynamical simulation. Both sets of authors again found that an area-scaling law was valid at low frequencies, namely, $A(\omega,h_0) \sim \omega^{\alpha} h_0^{\beta}$, with $\alpha \simeq 0.40$ and $\beta \simeq 0.47$. Furthermore, Acharyya and Chakrabarti [13,14] have also performed MC simulations of the Ising model in an oscillating field and have obtained scaling laws for the loop area over a wide range of values of h_0, ω, and temperature T.

The above discussion indicates that the loop area exhibits different scaling laws in different windows of (ω,h_0) space. This is clearly not satisfying and suggests that the above studies may be seeing only limited ranges of a more general behavior of the loop area $A(\omega,h_0)$. This is the approach emphasized by Sides *et al.* [15–17] in a comprehensive study of this problem. Essentially, these authors argue that the hysteresis loop in pure Ising systems (and the associated dynamical phase transitions) should be interpreted in terms of decay of metastable phases through nucleation and growth of (single or multiple) droplets. This leads to asymptotically logarithmic dependencies of $A(\omega,h_0)$ on ω and h_0. However, the modulations are extremely slow and $A(\omega,h_0)$ appears to exhibit power-law scaling even over a few decades of parameter values. Of course, the ''power-law'' exponents are dependent on the window of parameters one focuses upon. Sides *et al.* have also peformed extensive MC simulations of hysteresis in kinetic Ising models, which both guide and confirm their analytical arguments. We believe that the work of Sides *et al.* provides an overview of hysteresis in pure Ising systems, which systematizes the earlier observations of diverse exponents.

This discussion has attempted to provide a brief review of hysteresis effects in pure systems. We hope that the main thrust of various studies has been clarified, namely, to establish the functional dependence of the hysteresis loop area on various system parameters. The same attitude will also guide our subsequent investigations of hysteresis loops in spin glasses.

B. Disordered spin systems

Let us next consider some representative studies of hysteresis in disordered systems. Acharyya and Chakrabarti [14] have also studied the dilute Ising model in an oscillatory field. In particular, they examined the effects of increasing dilution on the area of the hysteresis loop. Their results are mostly qualitative, with the most relevant observation being that there is no unusual behavior as the density of spins goes through the percolation threshold. A similar observation holds in the context of the pure Ising model, where there are no dramatic effects as the temperature is varied through the critical temperature T_c. After all, there is no reason to expect signatures of an equilibrium phase transition in a nonequilibrium situation.

Another interesting work in this context is due to Sethna *et al.* [18], who studied hysteretic effects in the $T=0$ random-field Ising model. These authors primarily focused upon the universal nature of distribution of domain avalanches along the hysteresis loop and their relation to Barkhausen noise.

Many authors have also investigated hysteresis effects in spin glasses. Let us first discuss relevant experimental works. Most experimental studies have been in the SG phase, where a wide variation in the shapes of hysteresis loops has been categorized. Experimental results also exhibit a strong dependence on the magnetic history of the system, e.g., the loops are of different shapes depending on whether the system is prepared by ''zero-field cooling'' or ''field cooling'' [1]. We do not review here the range of experimentally observed hysteresis loops but merely provide some relevant references [19–22].

An early numerical study of this problem is due to Soukolis *et al.* [23,24], who conducted MC studies of hysteresis effects in (a) Ising spin glasses with long-ranged interactions [23], and (b) Heisenberg spin glasses with long-ranged exchange interactions and anisotropic Dzyaloshinsky-Moriya (DM) terms [24]. Both these studies were conducted in the SG phase. The results of Soukolis *et al.* can be summarized as follows:

(i) Hysteresis loops observed for the Ising glass with zero ferromagnetic bias are smooth and continuous—in qualitative agreement with results for dilute AuFe systems [19].

(ii) Sharp magnetization reversals are only observed for Ising glasses with strong ferromagnetic bias. In this case, the hysteresis loops are qualitatively similar to those seen for more concentrated AuFe systems [19], as well as CuMn and AgMn systems [21,22].

(iii) Displaced hysteresis loops were only observed for Heisenberg glasses. Experimentally, displaced loops are seen in glasses containing Mn under special preparation conditions [20–22].

Numerical studies of hysteresis effects in Heisenberg glasses have also been undertaken by Dasgupta and Yao [25], who also include anisotropy through the DM interaction. Dasgupta and Yao found that weak anisotropy effects promote the rigidity of the spin system during rotation and inversion of magnetization, and there is a decrease in the sharpness of the hysteresis loop with increasing anisotropy. This provides an independent mechanism for sharp magnetization reversals in hysteresis loops.

Finally, we mention a recent work by Pazmandi *et al.* [26], who studied hysteresis in $T=0$ Ising spin glasses with zero ferromagnetic bias. These authors numerically determined the distribution function of domain avalanches during the evolution. They demonstrate that this distribution exhibits ''self-organized critical'' behavior all along the hysteresis loop.

The above works have primarily confined themselves to qualitative statements about the shapes and sizes of hysteresis loops. In this paper, we undertake a quantitative numeri-

cal study of the dependence of the hysteresis loop area upon disorder for spin systems with long-ranged interactions. In particular, we present detailed numerical results for the dependence of the loop area on disorder. The results presented ere are obtained from simulations of a soft-spin version of the SK model for spin glasses.

III. THEORETICAL MODELING

The usual model for spin glasses (with long-ranged interactions) is the SK model [27] with the Hamiltonian:

$$H=-\sum_{\langle i,j\rangle}^{N} J_{ij}\sigma_i\sigma_j-h\sum_{i=1}^{N}\sigma_i, \tag{2}$$

where the magnetic impurities (N in number) are described by an Ising spin $\sigma_i=\pm 1$. In general, each spin interacts with all other spins (excluding itself) and the exchange interaction J_{ij} is chosen to be a random variable, introducing disorder and frustration in the model. It is customary to assume that the distribution of J_{ij} is Gaussian:

$$P(J_{ij})=\frac{1}{\sqrt{2\pi\tilde{J}^2}}\exp\left[-\frac{(J_{ij}-J_0)^2}{2\tilde{J}^2}\right], \tag{3}$$

where $\tilde{J}$ is the variance of the distribution, and $\langle J_{ij}\rangle=J_0$ is the ferromagnetic bias, which we always set to zero in this paper. The quantities J_0 and $\tilde{J}$ are scaled by N and $N^{1/2}$, respectively, to ensure that appropriate thermodynamic quantities are extensive in the $N\to\infty$ limit. In Eq. (2), h refers to an external magnetic field.

In this paper, we will focus upon the soft-spin version of the SK model with the Hamiltonian:

$$H=-\frac{\tilde{r}}{2}\sum_{i=1}^{N}\sigma_i^2+\frac{\tilde{u}}{4}\sum_{i=1}^{N}\sigma_i^4-\sum_{\langle i,j\rangle}^{N}J_{ij}\sigma_i\sigma_j-h\sum_{i=1}^{N}\sigma_i, \tag{4}$$

where σ_i is now a continuous variable with $\sigma_i\epsilon[-\infty,\infty]$. In Eq. (4), $\tilde{r}$ and $\tilde{u}$ are positive, phenomenological parameters and the two-state SK model is recovered in the limit $\tilde{r},\tilde{u}\to\infty$, with their ratio remaining finite. The soft-spin SK model has proven to be a convenient starting point for analytical calculations [28,29].

In the present case, we are interested in an explicitly time-dependent system with the magnetic field having an oscillatory form $h=h_0\cos(\omega t)$, where h_0 is the amplitude, and ω is the frequency. We associate dissipative dynamics with the SK Hamiltonian by coupling the system to a heat bath, which induces spin flips. For metallic spin glasses, this heat bath can be identified with conduction electrons, which produce single-spin flip processes with impurity spins via an exchange interaction. Since the spin-glass free-energy landscape has a large number of metastable states, the dynamics of the system is expected to be complicated. The metastable states are separated by activation barriers of varying heights. Therefore, it is possible to have thermally activated transitions leading to a broad distribution of relaxation times.

Dynamical properties of disordered systems have often been studied by MC simulations of the SK model in conjunction with spin-flip Glauber dynamics [1–4]. However, we focus upon dissipative Langevin dynamics associated with the corresponding soft-spin Hamiltonian as modeled by the usual TDGL formulation [30,31]:

$$\begin{aligned}\frac{d\sigma_i(t)}{dt}&=-\Gamma\frac{\delta(\beta H)}{\delta\sigma_i}+\xi_i(t)\\&=\Gamma\left[r\sigma_i-u\sigma_i^3+\beta\sum_{j=1(j\neq i)}^{N}J_{ij}\sigma_j+\beta h_0\cos(\omega t)\right]+\xi_i(t).\end{aligned} \tag{5}$$

In Eq. (5), Γ^{-1} is the time scale of individual spin flips; and we have introduced $r=\beta\tilde{r}$; $u=\beta\tilde{u}$, where $\beta=(k_BT)^{-1}$ is the inverse temperature. The effect of the heat bath is represented by the Gaussian random noise term $\xi_i(t)$ driving the system, which is characterized by

$$\begin{aligned}\langle\xi_i(t)\rangle&=0,\\\langle\xi_i(t)\xi_j(t')\rangle&=2\Gamma\delta_{ij}\delta(t-t').\end{aligned} \tag{6}$$

The angular brackets in Eq. (6) represent an averaging over the thermal noise ensemble, and the fluctuation-dissipation condition on the variance ensures a proper equilibrium distribution.

Before we proceed, we should stress that the Langevin approach has several advantages over the MC approach. First, there is an intrinsic averaging involved at the level of defining variables (or order parameters) in the Langevin formulation. This enables us to obtain smooth and conclusive numerical results with considerably less numerical effort than in the MC approach. Secondly, MC simulations may become considerably time consuming because the system can get stuck for a long time in a single valley if the neighboring free-energy barriers are too high—particularly at low temperatures. (Of course, this may be true for the Langevin model also, especially at weak values of h_0. Nevertheless, the continuous spins have more routes to relax from metastable states in comparison to ''hard'' MC spins.) Finally, the SK model with Glauber kinetics is analytically intractable, whereas the corresponding continuum model is amenable to approximate analytical solution.

It is convenient to rescale variables in Eq. (5) so as to reduce the number of free quantities. We introduce the rescaled variables:

$$\begin{aligned}\sigma_i'&=\sqrt{\frac{u}{r}}\sigma_i,\\t'&=\Gamma t,\\J_{ij}'&=\beta J_{ij},\\\tilde{J}'&=\beta\tilde{J},\\h_0'&=\beta h_0\sqrt{\frac{u}{r}},\\\omega'&=\frac{\omega}{\Gamma},\end{aligned} \tag{7}$$

and obtain the dimensionless dynamical equation (dropping primes):

$$\frac{d\sigma_i(t)}{dt} = r(\sigma_i - \sigma_i^3) + \sum_{j=1,(j\neq i)}^{N} J_{ij}\sigma_j + h_0\cos(\omega t) + \eta_i(t). \tag{8}$$

In all subsequent discussions, we will always refer to dimensionless variables only. In Eq. (8), the distribution of the exchange coupling J_{ij} is obtained as

$$P(J_{ij}) = \frac{1}{\sqrt{2\pi\tilde{J}^2}}\exp\left[-\frac{J_{ij}^2}{2\tilde{J}^2}\right], \tag{9}$$

where the variance $\tilde{J}$ must be scaled by $N^{1/2}$, i.e., $\tilde{J} = JN^{-1/2}$, where J is independent of N. The rescaled Gaussian white noise $\eta_i(t)$ is defined by

$$\langle \eta_i(t)\rangle = 0,$$

$$\langle \eta_i(t)\,\eta_j(t')\rangle = 2\frac{u}{r}\delta_{ij}\delta(t-t'). \tag{10}$$

Equations (8)–(10) constitute the dynamical model that we investigate in the present paper. It should be kept in mind that, in the corresponding two-state model (which arises for $r,u\to\infty$ and $h_0=0$), the transition between the paramagnetic and spin-glass states occurs at $\beta J=1$. In the present case, the transition point will depend upon r and u, in general.

IV. DETAILED NUMERICAL RESULTS

Our numerical study focused upon qualitative and quantitative properties of hysteresis loops in spin-glass systems. In particular, we investigated the shape and area of the hysteresis loop as a function of both disorder and the applied field—characterized by a field strength h_0 and frequency ω. We have considered cases with (a) ''weak'' disorder, where the $h=0$ system is in the paramagnetic state, and (b) ''strong'' disorder, where the $h=0$ system is in the SG state.

We integrated Eqs. (8)–(10) using an Euler discretization scheme with very fine mesh size $\Delta t = 10^{-4}$. We have confirmed that numerical results are unchanged on further reduction of the mesh size. We should remark here that considerably higher values of Δt also give qualitatively reasonable results. However, we have preferred to simulate the model in a ''continuum limit'' so as to avoid discreteness effects, which may interfere with the delicate effects of disorder. Typically, the simulations were carried out on a system of size $N=100$ spins. We also did some trial simulations with $N=200$ spins and the results were numerically indistinguishable from those for $N=100$ spins. The initial configuration for each run was chosen to be a random mixture of $+1$ and -1 with equal probability.

For the results shown in this paper, some parameters in Eqs. (8)–(10) are fixed, namely, $r=u=2.0$ and $h_0=10.0$. We present results for a range of values of J and ω. We have also investigated other values of r,h_0 and the results presented here are representative of results for a wide range of (r,h_0) values. Finally, thermal noise was mimicked by Gaussian random numbers with the appropriate amplitude. The hysteresis loop area $\oint m(t)dh(t)$ [where $m(t)$ is the time-dependent average magnetization] was computed after allowing the initial configuration to equilibrate into a stable loop, which typically took 15 field cycles. All statistical data was obtained as an average over at least 40 sets of initial conditions for each disorder configuration. In addition, the data was averaged over at least 40 disorder configurations. Wherever necessary, even further averaging was performed to improve data quality.

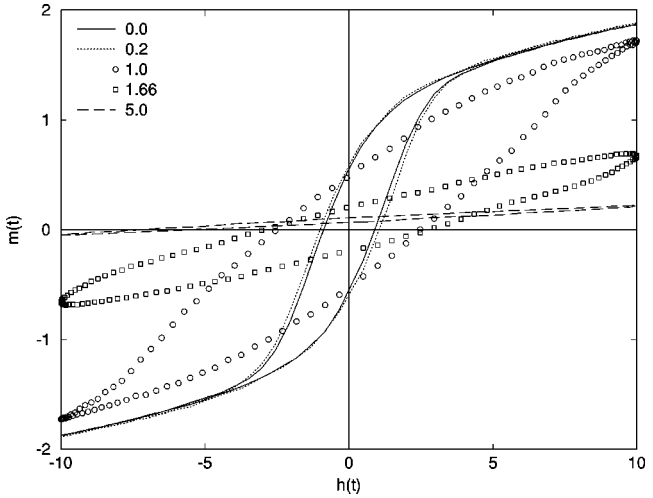

FIG. 1. Effects of disorder amplitude (J) on the shapes of hysteresis loops. We plot the time-dependent magnetization $m(t)$ vs the magnetic field $h(t)$ for $J=0.0$, 0.2, 1.0, 1.66, and 5.0—denoted by the specified line types and symbols. The amplitude and frequency of the magnetic field were fixed at $h_0=10.0$ and $\omega=0.1$. Other details of the simulation are described in the text.

Figures 1 and 2 summarize the qualitative effects of dis-

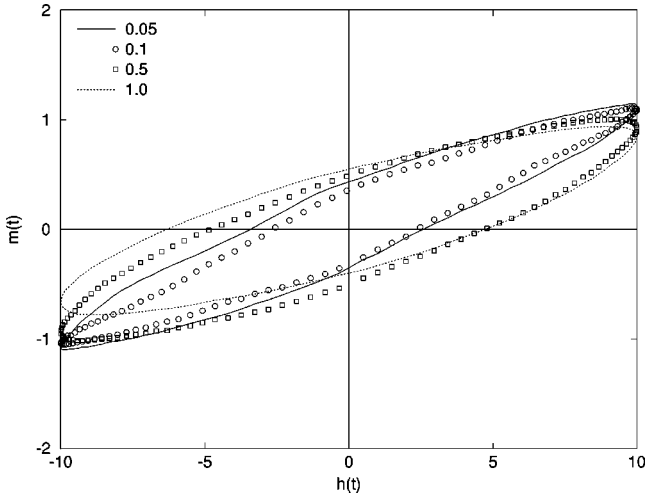

FIG. 2. Effects of frequency (ω) on the shapes of hysteresis loops. We present data for $\omega=0.05$, 0.1, 0.5, 1.0—denoted by the specified line types and symbols. The disorder amplitude was fixed at $J=1.25$.

order on the shapes of hysteresis loops for a single field cycle. Figure 1 shows results for disorder amplitudes $J=0.0$, 0.2, 1.0, 1.66, and 5.0, with the frequency fixed at $\omega=0.1$. In the absence of an applied field, the system is in the paramagnetic phase for $J=0.0$ and 0.2, and in the SG phase for $J=1.0$, 1.66, and 5.0. There are two primary effects of increasing disorder on the shape of the hysteresis loop. The first important feature is the dependence of the slope of the loops on disorder amplitude. The $J=0$ case corresponds to the limit of disconnected spins [6–8], which exhibit a relatively rapid response to a sign change in the external field. The nature of this response is determined by a comparison of the spin-relaxation time (τ_r) with the inverse frequency (ω^{-1}). Typically, $\tau_r \ll \omega^{-1}$ corresponds to the low-hysteresis limit, as the spin readjusts to the applied field before it changes substantially.

If the disorder amplitude is increased, the free-energy surface becomes complicated and is characterized by multiple metastable minima, differing from each other by small groups of spins. In the absence of an external field, there is a distribution of barrier heights ($\mathbf{\Delta}$); and a corresponding distribution of escape times from these minima ($\tau_e \sim e^{\beta \mathbf{\Delta}}$). To the best of our knowledge, there is no rigorous calculation of the barrier distribution as a function of J and N [1–4]. A rough estimate of barrier heights can be obtained as follows. Typically, configurations in the free-energy landscape differ by clusters of $O(N^{1/2})$ spins [4], with an associated barrier energy $\mathbf{\Delta} \sim N^{1/4} J$ in the SK model. The MC simulations of Mckenzie and Young [32] demonstrate that the barrier distribution is approximately uniform up to this level. In the presence of a constant magnetic field h, the energy associated with a spin cluster is $\mathbf{\Delta}_h \sim N^{1/4} h$. Therefore, the relevant parameter to understand relative effects of disorder and magnetic field is $\mathbf{\Delta}/\mathbf{\Delta}_h \sim J/h$.

Next, consider the effect of a time-dependent magnetic field $h(t)=h_0 \cos(\omega t)$ in the following cases : (a) If $h_0 \gg \mathbf{\Delta}$, the hysteretic response will be unaffected by the disorder when $|h(t)| \simeq h_0$. The only effects of disorder are seen when $h(t) \simeq 0$, and the range of relevant escape times are determined by $\omega^{-1} > \tau_e$. Thus, we expect diminishing effects of disorder as ω is increased. (We will quantify this shortly.) (b) If $h_0 \sim \mathbf{\Delta}$, similar arguments apply except that the effects of disorder are seen through the entire hysteresis cycle. (c) If $h_0 \ll \mathbf{\Delta}$, the effects of disorder are dominant and temporal evolution occurs primarily through thermally activated barrier hopping. In this limit, we do not even expect well-defined hysteresis loops.

The hysteresis loops in Fig. 1 bear out the above arguments. For $J<0.2$, the hysteresis loops are barely distinguishable from that for $J=0$. The only differences are seen in the region where $h(t) \sim 0$. This difference also diminishes as ω increases, as we will quantify shortly. At higher amplitudes of disorder, trapping of the system in metastable states prevents sharp reversal of spins. Therefore, the slopes of the hysteresis loops become increasingly flatter with increase in disorder. Even more drastic effects of trapping are seen for stronger disorder, e.g., the loop for $J=5.0$, which is actually displaced from the origin—a consequence of long-term trapping in a restricted region of phase space. In some cases, we observe that the hysteresis loops do not always close on completion of a field cycle. Finally, for extremely large values of disorder, the system is unable to respond to the changing field. Clearly, there will be no hysteresis loops for infinite disorder amplitude, since the driving field will be unable to remove the system from a trapped state.

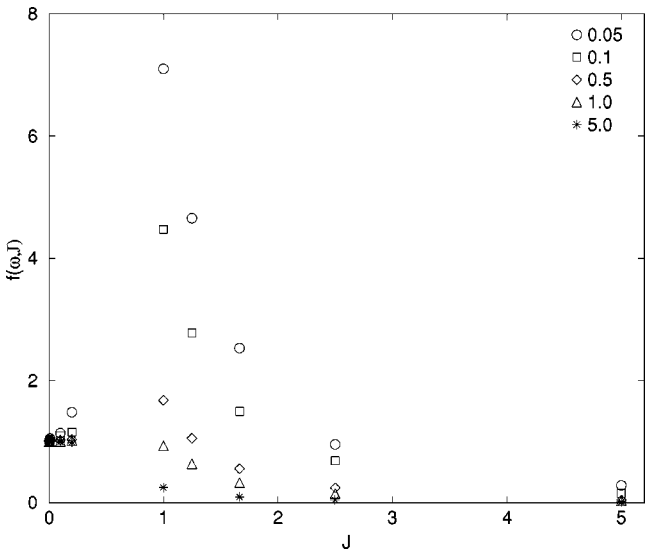

FIG. 3. Plot of $f(\omega,J)$ $[=A(\omega,J)/A(\omega,0)]$ vs J for a wide range of disorder amplitudes. The quantity $A(\omega,J)$ is the area of the hysteresis loop for frequency ω and disorder amplitude J. We present data for $\omega=0.05$, 0.1, 0.5, 1.0, and 5.0—denoted by the specified symbols.

The second important feature concerns the tails of the loops, which become more open (relative to the width at zero field) for larger disorder values. Correspondingly, the shapes of the loops also become more elliptical as the disorder amplitude is increased. This should be contrasted with tails in systems with no disorder (or weak disorder), where the saturation magnetization is attained rapidly. The results in Fig. 1 are consistent with those from earlier numerical simulations [23], and also experimental results [19,22].

Figure 2 shows hysteresis loops for field frequency $\omega=0.05$, 0.1, 0.5, and 1.0, for a representative value of the disorder amplitude $J=1.25$. The loops become flatter at higher frequencies. As we demonstrate shortly, the effects of disorder are diminished with increasing frequency when $h_0 \geqslant \mathbf{\Delta}$.

We next attempt to quantify the effects of disorder on the area of the hysteresis loop. As we have stressed in Sec. II, this experimentally relevant quantity has been the subject of most investigations. It is convenient to focus on the quantity

$$f(\omega,J)=\frac{A(\omega,J)}{A(\omega,0)}, \tag{11}$$

where $A(\omega,J)$ is the area of the hysteresis loop at frequency ω and disorder amplitude J; with other parameters being fixed as specified earlier. Clearly, $f(\omega,0)=1$, so the strong dependence of $A(\omega,0)$ on ω [6–8] has been factored out in our definition.

Figure 3 plots $f(\omega,J)$ vs J for a wide range of disorder

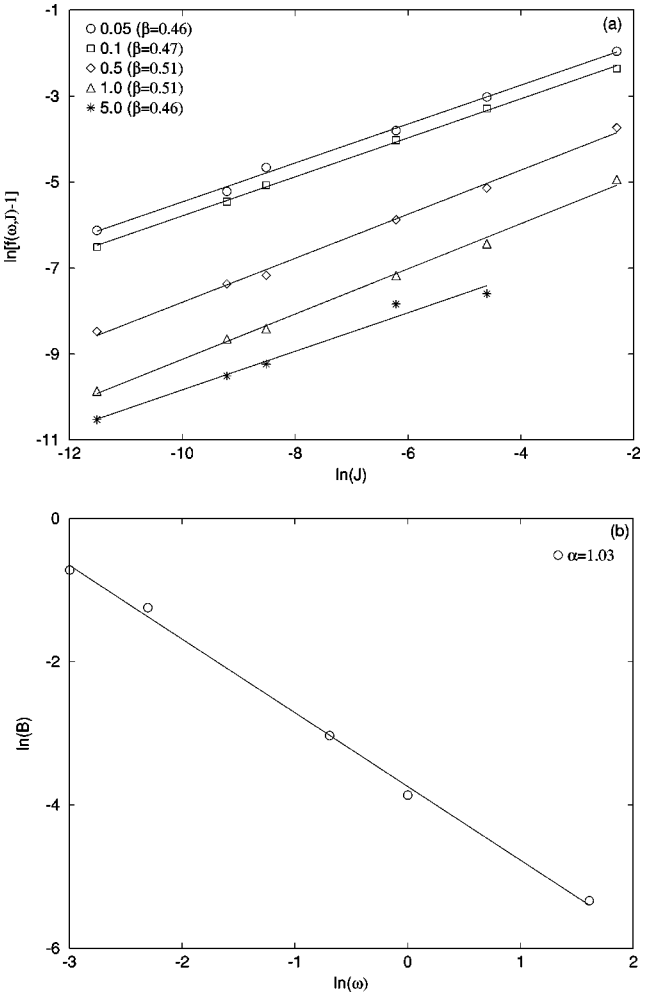

FIG. 4. (a) Plot of $\ln[f(\omega,J)-1]$ vs $\ln(J)$ over 4 decades of weak disorder values, ranging from $J=10^{-5}$ to $J=10^{-1}$. We present data for $\omega=0.05$, 0.1, 0.5, 1.0, and 5.0—denoted by the specified symbols. The best linear fits are superposed on the relevant data sets, and the corresponding exponents (referred to as β in the text) are specified in the figure. The error bars on exponent values are ± 0.01. (b) Plot of $\ln(B)$ vs $\ln(\omega)$, where $\ln(B)$ is obtained as the intercept of the appropriate best-fit line in Fig. 4(a). The best-fit line for the present data set is shown in the figure, and the relevant exponent is $\alpha=1.03\pm 0.01$.

values and for frequencies $\omega=0.05$, 0.1, 0.5, 1.0, and 5.0. We will shortly examine the behavior of $f(\omega,J)$ in various limits, but it is useful to make some general observations as follows: (a) As expected, $f(\omega,0)=1$ and $f(\omega,\infty)=0$. (b) The function $f(\omega,J)$ rises to a maximum at $J=J_m$ and then decays to 0. The quantity $f(\omega,J_m)$ decreases with increasing frequency. (c) In general, $f(\omega,J)$ decreases with increasing frequency.

Let us now elucidate various limiting behaviors of the function $f(\omega,J)$. Figure 4(a) plots $\ln[f(\omega,J)-1]$ vs $\ln(J)$ from Fig. 3 for weak values of disorder, ranging from $J=10^{-5}$ to $J=10^{-1}$. In the absence of a magnetic field, these values of disorder correspond to the paramagnetic phase. Figure 4(a) constitutes strong numerical evidence of a power-law scaling $f(\omega,J)\simeq 1+B(\omega)J^{\beta}$, which holds over four decades of disorder amplitude. The best-fit values for β are specified in the figure and appear to be universal. The suggested universal exponent is (obviously) $\beta=1/2$, but we have no theoretical argument for such a behavior.

Next, we consider the behavior of $f(\omega,J)$ with ω. Figure 4(b) plots $\ln(B)$ vs $\ln(\omega)$, obtained from the best-fit lines in Fig. 4(a). Again, the data exhibits a reasonable power-law scaling, $B(\omega)\simeq b\omega^{-\alpha}$, albeit over two decades of frequency. The best-fit value for this exponent is $\alpha=1.03\pm 0.01$. Combining the results of Figs. 4(a) and 4(b), we obtain an overall scaling form for $f(\omega,J)$ as

$$f(\omega,J)\simeq 1+b\omega^{-\alpha}J^{\beta}+\text{higher order terms}, \qquad (12)$$

valid for the weak values of disorder considered here. Equation (12) is the main result of this paper. We again stress that we have no analytical arguments to support this functional form. Nevertheless, the numerical evidence is rather compelling, and we hope our results will provoke further numerical and analytical investigations of this problem. Furthermore, in the context of the arguments by Sides *et al.* [15,16] in the case of pure systems, we have no strong reason to believe that the power laws in Eq. (12) are universal. It is reasonable to believe that the form of Eq. (12) may be only a limiting case of a more general expression—even though it appears to hold for an extended range of parameter values. Of course, the elucidation of such behavior must necessarily rely upon analytic arguments, which are not available at present.

Let us now consider stronger values of disorder, corresponding to the SG phase in the absence of a magnetic field. Figure 5(a) plots $\ln[f(\omega,J)]$ vs $\ln(J)$ for values of disorder ranging from $J=1.0$ to $J=5.0$; and frequencies $\omega=0.05$, 0.1, 0.5, 1.0, and 5.0. We should stress again that hysteresis loops are not well-defined at much higher values of disorder. For example, the effects of Barkhausen noise, which arise due to avalanches all along the hysteresis loop [26], are more pronounced at high disorder values. Furthermore, as we have remarked earlier, the loops may not even close at high values of disorder. Over the limited range of disorder values for which reliable data is available, the data for $f(\omega,J)$ again exhibits a reasonable power-law scaling $f(\omega,J)\simeq C(\omega)J^{-\delta}$. The best-fit exponents for different values of frequency are shown in the figure, and again appear to be universal. Figure 5(b) plots $\ln(C)$ vs $\ln(\omega)$, where $\ln(C)$ is obtained from the best-fit lines in Fig. 5(a). Again, the data exhibits a reasonable power-law behavior $C(\omega)\simeq c\omega^{-\gamma}$ over two decades of frequency. The results from Figs. 5(a) and 5(b) suggest an overall scaling form $f(\omega,J)\simeq b\omega^{-\gamma}J^{-\delta}$, valid for strong disorder values—though the numerical evidence for this form is not as compelling as that for Eq. (12).

We have also studied the remnant magnetization $m_r(\omega,J)$ [i.e., the width of the hysteresis loop when $h(t)=0$]; and the saturation magnetization $m_s(\omega,J)$ (i.e., the maximum magnetization in the cycle). We should remark that the saturation value of the magnetization need not necessarily occur when $h(t)$ is maximum—especially for strong disorder values. At weak values of disorder [as in Fig. 4(a)], it is not possible to clearly distinguish the values of $m_r(\omega,J)$ and $m_s(\omega,J)$ from the corresponding values at $J=0$. This is due to the

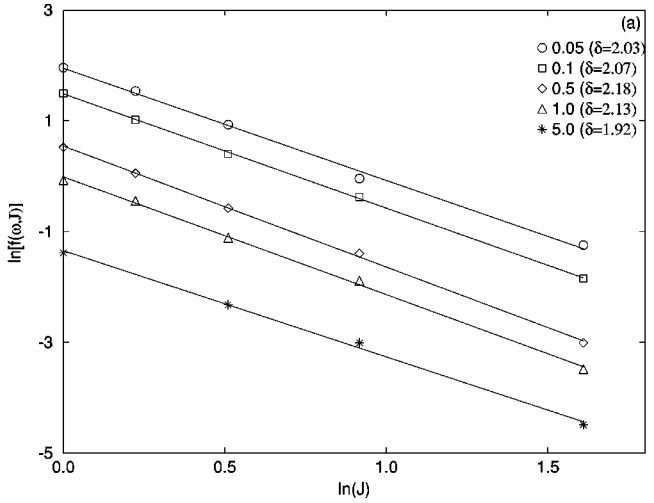

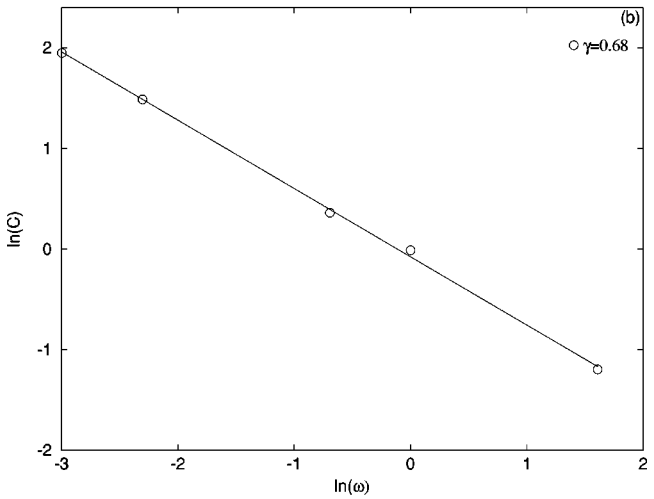

FIG. 5. (a) Plot of $\ln[f(\omega,J)]$ vs $\ln(J)$ for strong disorder values, ranging from $J=1.0$ to $J=5.0$. We present data for $\omega=0.05$, 0.1, 0.5, 1.0, and 5.0—denoted by the specified symbols. The best linear fits are superposed on the relevant data sets, and the corresponding exponents (referred to as δ in the text) are specified in the figure. The error bars on exponent values are ± 0.01. (b) Plot of $\ln(C)$ vs $\ln(\omega)$, where $\ln(C)$ is obtained as the intercept of the appropriate best-fit line in Fig. 5(a). The corresponding best-fit line for the present data set is shown in the figure, and the relevant exponent is $\gamma=0.68\pm 0.01$.

Barkhausen noise along the hysteresis curve, whose amplitude is comparable to the differences $|m_i(\omega,J)-m_i(\omega,0)|$, $i\equiv r,s$.

For strong disorder [as in Fig. 5(a)], we obtain clear numerical results for these quantities. Figure 6 plots $\ln[m_i(\omega,J)/m_i(\omega,0)]$ vs $\ln(J)$ for strong disorder and $\omega=0.1$. The scaling form of the remnant magnetization is similar to that shown for $f(\omega,J)$ in Fig. 5. This is trivially understood if the hysteresis loop is approximated as an ellipse. However, due to trapping and saturation effects in the tails of the loops, the saturation magnetization does not exhibit simple scaling behavior, as seen in Fig. 6.

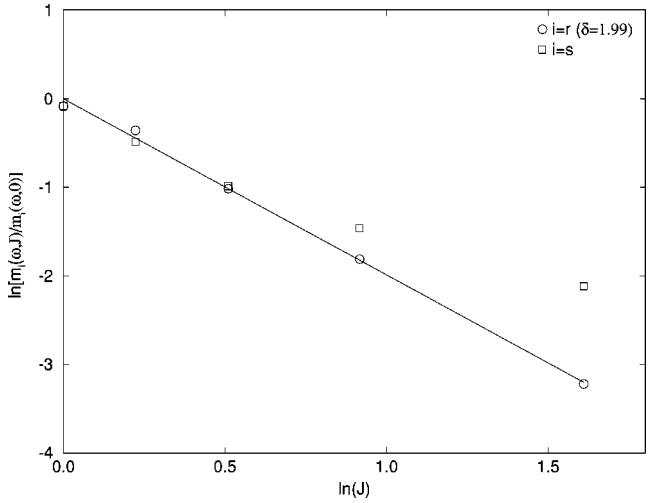

FIG. 6. Plot of $\ln[m_i(\omega,J)/m_i(\omega,0)]$ vs $\ln(J)$ for strong disorder. The labels $i=r$ and $i=s$ refer to the ''remnant magnetization'' and ''saturation magnetization,'' respectively. The best-fit line to the remnant magnetization data is superposed on the relevant data set and the best-fit exponent is $\delta=1.99\pm 0.01$.

V. SUMMARY AND DISCUSSION

Let us briefly summarize the results presented in this paper. We have undertaken a detailed numerical study of hysteresis loops in spin systems with quenched disorder in the exchange interactions, and zero ferromagnetic bias. In particular, we have focused on the variation of the loop area as a function of disorder amplitude (J) and field frequency (ω). The loop area is the most important experimental characteristic of the hysteresis loop, as it measures the heat dissipated in a field cycle.

For weak values of disorder, where the system is paramagnetic in the absence of a magnetic field, we find compelling numerical evidence for power-law scaling of the quantity $f(\omega,J)=A(\omega,J)/A(\omega,0)$, where $A(\omega,J)$ is the loop area at frequency ω and disorder amplitude J. The power-law scaling is seen for four decades of disorder and two decades of frequency. At present, we have no analytical arguments to support this scaling form but hope that our numerical results will provide an impetus for further investigations of this problem.

For strong values of disorder, where the system is in the spin-glass phase in the absence of a magnetic field, we also observe power-law scaling of $f(\omega,J)$. However, this applies only for a restricted range of disorder values. We do not have results for very high disorder amplitudes, where there are no well-defined hysteresis loops. We have also studied other relevant quantities like the remnant and saturation magnetizations of the hysteresis loop.

Qualitatively, the effects of disorder on hysteresis loops can be understood in terms of a semiphenomenological model involving clusters of a small number of spins [33,23]. This model invokes the properties of the free-energy surface of a disordered system, which is comprised of metastable minima separated by barriers. The free-energy surface is

comprised of a distribution of barrier heights (Δ), and a consequent distribution of escape times from the metastable minima (τ_e). For magnetic-field strengths, $h_0 \geqslant \Delta$, we expect that the escape times that are relevant to spin dynamics in an oscillatory magnetic field, satisfy $\omega^{-1} > \tau_e$. Therefore, we expect the effects of disorder to be diminished at higher-field frequencies—in accordance with our numerical results.

Of course, the simple argument above only serves to establish trends. At present, we are attempting to quantify these arguments with the goal of providing an analytical basis for the scaling laws suggested by our numerical simulations. At least in the context of weak disorder, where the field-free system is paramagnetic, we believe that it will be possible to formulate the necessary arguments.

ACKNOWLEDGMENTS

The authors are grateful to C. Dasgupta for a critical reading of this manuscript, giving us a number of valuable suggestions, and bringing Ref. [25] to our notice. We are also grateful to M. Novotny for a careful criticism of this manuscript.

[1] K. Binder and A.P. Young, Rev. Mod. Phys. **58**, 801 (1986); and references therein.
[2] *Heidelberg Colloquium on Glassy Dynamics*, edited by J.L. van Hemmen and I. Morgenstern, Lecture Notes in Physics Vol. 275 (Springer, Berlin, 1986), and references therein.
[3] M. Mezard, G. Parisi, and M.A. Virasoro, *Spin Glass Theory and Beyond* (World Scientific, Singapore, 1987), and references therein.
[4] K.H. Fischer and J.A. Hertz, *Spin Glasses* (Cambridge University Press, Cambridge, 1991), and references therein.
[5] G.S. Agarwal and S.R. Shenoy, Phys. Rev. A **23**, 2719 (1981); S.R. Shenoy and G.S. Agarwal, *ibid.* **29**, 1315 (1984).
[6] P. Jung, G. Gray, R. Roy, and P. Mandel, Phys. Rev. Lett. **65**, 1873 (1990).
[7] D. Bose and S. Sarkar, Phys. Rev. E **56**, 6581 (1997).
[8] D. Bose and S. Sarkar, Phys. Lett. A **232**, 49 (1997); S. Sarkar and D. Bose, Phys. Rev. E **58**, 5471 (1998).
[9] M. Rao, H.R. Krishnamurthy, and R. Pandit, Phys. Rev. B **42**, 856 (1990); J. Phys.: Condens. Matter **1**, 9061 (1991).
[10] D. Dhar and P. Thomas, J. Phys. A **25**, 4967 (1992).
[11] W.S. Lo and R.A. Pelcovits, Phys. Rev. A **42**, 7471 (1990).
[12] S. Sengupta, Y.J. Marathe, and S. Puri, Phys. Rev. B **45**, 7828 (1992).
[13] M. Acharyya and B.K. Chakrabarti, Physica A **192**, 471 (1993); **202**, 467 (1994).
[14] M. Acharyya and B.K. Chakrabarti, in *Annual Reviews of Computational Physics*, Vol. 1, edited by D. Stauffer (World Scientific, Singapore, 1994).
[15] S.W. Sides, P.A. Rikvold, and M.A. Novotny, Phys. Rev. E **57**, 6512 (1998).
[16] S.W. Sides, P.A. Rikvold, and M.A. Novotny, Phys. Rev. Lett. **81**, 834 (1998); Phys. Rev. E **59**, 2710 (1999); J. Appl. Phys. **83**, 6494 (1998).
[17] P.A. Rikvold, G. Korniss, C.J. White, M.A. Novotny, and S.W. Sides, e-print cond-mat/9904028 (unpublished).
[18] J.P. Sethna, K. Dahmen, S. Kartha, J.P. Krumhansl, B.W. Roberts, and J.D. Shore, Phys. Rev. Lett. **70**, 3347 (1993); O. Perkovic, K. Dahmen, and J.P. Sethna, *ibid.* **75**, 4528 (1995).
[19] R.J. Borg and T.A. Kitchens, J. Phys. Chem. Solids **34**, 1323 (1973).
[20] P.A. Beck, Prog. Mater. Sci. **23**, 1 (1978).
[21] P. Monod, J.J. Prejean, and B. Tissier, J. Appl. Phys. **50**, 7324 (1979).
[22] J.J. Prejean, M. Joliclerc, and P. Monod, J. Phys. (Paris) **41**, 427 (1980).
[23] C.M. Soukoulis, K. Levin, and G.S. Grest, Phys. Rev. Lett. **48**, 1756 (1982); Phys. Rev. B **28**, 1495 (1983).
[24] C.M. Soukoulis, G.S. Grest, and K. Levin, Phys. Rev. Lett. **50**, 80 (1983); Phys. Rev. B **28**, 1510 (1983).
[25] C. Dasgupta and K.-L. Yao, Phys. Rev. B **29**, 4071 (1984).
[26] F. Pazmandi, G. Zarand, and G.T. Zimanyi, Phys. Rev. Lett. **83**, 1034 (1999).
[27] D. Sherrington and S. Kirkpatrick, Phys. Rev. Lett. **35**, 1792 (1975); Phys. Rev. B **17**, 4384 (1978).
[28] J.A. Hertz and R.A. Klemm, Phys. Rev. B **20**, 316 (1979).
[29] H. Sompolinsky and A. Zippelius, Phys. Rev. Lett. **47**, 359 (1981); Phys. Rev. B **25**, 6860 (1982).
[30] S.K. Ma, *Modern Theory of Critical Phenomena* (Benjamin, New York, 1976).
[31] P.C. Hohenberg and B.I. Halperin, Rev. Mod. Phys. **49**, 435 (1977).
[32] N.D. Mackenzie and A.P. Young, Phys. Rev. Lett. **49**, 301 (1982); J. Phys. C **16**, 5321 (1983).
[33] C. Dasgupta, S.K. Ma, and C.H. Hu, Phys. Rev. B **20**, 3837 (1979).